Equatorial jets in decaying shallow-water turbulence on a rotating sphere

Yuji Kitamura[*] and **Keiichi Ishioka**

Division of Earth and Planetary Sciences, Graduate School of Science,

Kyoto University, Kyoto, 606-8501, Japan.

November 29, 2006

[*] kitamura@kugi.kyoto-u.ac.jp

Abstract

Ensemble experiments of decaying shallow-water turbulence on a rotating sphere are performed to confirm the robustness of emergence of an equatorial jet. While previous studies have reported that the equatorial jets emerging in shallow-water turbulence are always retrograde, predominance of a prograde jet, although less likely, was also found in the present ensemble experiments. Furthermore, a zonal-mean flow induced by wave-wave interactions was examined using a weak nonlinear model to investigate the acceleration mechanisms of the equatorial jet. The second-order acceleration is induced by the Rossby and mixed Rossby-gravity waves and its mechanisms can be categorized into two types. First, the local meridional wavenumber of a Rossby wave packet propagating toward the equator increases due to meridional variation of the Rossby deformation radius and/or the retrograde zonal-mean flow, resulting in a dissipation of the wave packet in the equatorial region. This mechanism always contributes to retrograde acceleration of an equatorial jet. Another mechanism is derived from the tilting of equatorial waves due to meridional shear of the zonal-mean flow. In this case, zonal-mean flow acceleration contributes to the intensification of a given basic flow.

1. Introduction

It is known that two-dimensional turbulence possesses different aspects from three-dimensional turbulence. Unlike 3D turbulence, vortices of the same sign tend to merge and spontaneously form a larger flow structure in 2D turbulence (Lilly 1969; McWilliams 1984). Since quasi-geostrophic turbulence, which is approximately valid in atmospheric motions on synoptic scales, is analogous to 2D turbulence (Charney 1971), knowledge for 2D turbulence on a rotating plane provides the fundamentals for examining large-scale structures of atmospheric motions. 2D turbulence and its rotational effects have been studied to investigate the nonlinear dynamics in the atmosphere and ocean by many authors.

Rhines (1975) firstly found that a zonal structure spontaneously becomes dominant in 2D turbulence on a β plane. The meridional scale of the zonal jet is characterized by the scale $L_\beta = \sqrt{2U_0/\beta}$ (U_0: a representative velocity) called the Rhines scale, in which the order between the linear and nonlinear terms is comparable. His pioneering study has motivated studies of rotating 2D turbulence as a problem of pattern formation. Vallis and Maltrud (1993) showed that the wave-turbulence boundary in wavenumber space has the smallest meridional wavenumber at the $k_x = 0$ axis (k_x: zonal wavenumber) due to the anisotropy of the frequency of Rossby waves and elucidated the mechanism for the predominance of zonally elongated structures, and their theory is extended to spherical geometry (Nozawa and Yoden 1997; Hayashi et al. 2000; Huang et al. 2001). Williams (1978) performed numerical simulations of forced 2D turbulence in a spherical geometry as a conceptual model in order to investigate the formation mechanisms for the band structure observed in the Jovian atmosphere and succeeded in reproducing alternative zonal jets. However, in his experiment, longitudinal periodicity and equatorial symmetry were assumed due to restrictions on the available computational resources. Yoden and Yamada (1993) conducted

numerical experiments of decaying 2D turbulence on a rotating sphere using a model covering a full spherical domain. They found that a retrograde circumpolar vortex emerges at high planetary rotation speeds, and that it is a robust feature in 2D turbulence on a rotating sphere that appears independently of the initial state.

The shallow-water equations are commonly adopted as the simplest model for considering the effects of divergence (Farge and Sadourny 1989; Yuan and Hamilton 1994). Cho and Polvani (1996) performed numerical experiments of shallow-water turbulence on a rotating sphere and found that a characteristic flow pattern emerges in shallow-water turbulence that is remarkably different from that in 2D nondivergent turbulence. In particular, an equatorial jet appears due to the effects of planetary rotation, instead of a polar jet which is dominant in 2D turbulence. They investigated the dependence of the magnitude and width of the equatorial jet on planetary rotation and on the Rossby deformation radius. They concluded that the equatorial jet becomes stronger and narrower with decreasing deformation radius and that its direction is always retrograde. However, they did not examine the robustness of these conclusions using various initial fields, and it still remains to be seen how much the direction and amplitude of the equatorial jet depend on the initial field. Moreover, they discussed neither what the formation and sustaining mechanisms may be nor why only a retrograde jet appears. Although Iacono et al. (1999) attributed the predominance of a retrograde jet to asymmetry between a cyclone and anticyclone in the shallow-water system, their interpretation seems insufficient for understanding why a retrograde jet concentrates in the equatorial region. While the cyclone-anticyclone asymmetry is more remarkable at higher latitudes where the Rossby numbers are smaller, the concentration of vorticity skewness in the equatorial region is more important for the generation of a retrograde equatorial jet.

As mentioned above, the issue of understanding the predominance of an equatorial jet in

shallow-water turbulence still remains. First, we will focus on the equatorial jet emerging in a decaying shallow-water turbulence on a rotating sphere; ensemble experiments with various initial states are performed and dependence of direction and magnitude of the equatorial jet on the initial state is investigated in order to confirm the robustness of the results reported by Cho and Polvani (1996). Second, we will examine the acceleration of a zonal-mean flow induced by wave-wave interactions with a linearized shallow-water model and discuss whether or not the formation and sustaining mechanisms of the equatorial jet obtained in the full nonlinear model can be explained in terms of the weak nonlinear framework.

This paper is organized as follows. In Section 2, ensemble experiments using the full nonlinear model will be described. The distribution of magnitude of a zonal flow at the equator will be used to investigate the dependency on initial states. We will discuss what characterizes the magnitude and width of an equatorial jet in a quasi-equilibrium state. Section 3 will describe the jet acceleration induced by waves and the acceleration mechanisms in terms of the weak nonlinear framework. Our concluding remarks will be given in Section 4.

2. Ensemble experiments using the full nonlinear model

2a. *Model description*

A set of shallow-water equation on a sphere is described in nondimensional form as follows:

$$\frac{\partial \zeta}{\partial t} = -\frac{1}{1-\mu^2}\left[\frac{\partial}{\partial \lambda}\left(f+\zeta\right)U + (1-\mu^2)\frac{\partial}{\partial \mu}\left(f+\zeta\right)V\right] + \nu_{2p}(-1)^{p+1}\Delta^p \zeta, \tag{1}$$

$$\frac{\partial D}{\partial t} = \frac{1}{1-\mu^2}\left[\frac{\partial}{\partial \lambda}\left(f+\zeta\right)V - (1-\mu^2)\frac{\partial}{\partial \mu}\left(f+\zeta\right)U\right] - \Delta\left(\frac{\Phi'}{\mathrm{Fr}^2} + \frac{U^2+V^2}{2(1-\mu^2)}\right) + \nu_{2p}(-1)^{p+1}\Delta^p D, \tag{2}$$

$$\frac{\partial \Phi'}{\partial t} = -\frac{1}{1-\mu^2}\left[\frac{\partial}{\partial \lambda}\left(U\Phi'\right) + (1-\mu^2)\frac{\partial}{\partial \mu}\left(V\Phi'\right)\right] - D + \nu_{2p}(-1)^{p+1}\Delta^p\Phi', \tag{3}$$

where λ is the longitude, $\mu(=\sin\theta)$ the sine latitude, t time, p the order of hyperviscosity, ν_{2p} the hyperviscosity coefficient, $f(=\mu/\mathrm{Ro})$ nondimensional planetary vorticity, Δ horizontal Laplacian, ζ the vertical component of vorticity, D horizontal divergence, Φ' geopotential anomaly, and $(U,V) = (u,v)\sqrt{1-\mu^2}$ (u and v are zonal and meridional velocity components, respectively). These equations are characterized by the two nondimensional parameters: Rossby number $\mathrm{Ro} = U_0/2a\Omega$ and Froude number $\mathrm{Fr} = U_0/\sqrt{\Phi_0}$. Here, U_0 is the representative velocity scale, a the radius of the sphere, Ω the planetary angular velocity, and Φ_0 the mean value of geopotential. No forcing term is included in the equations, because our focus is on decaying turbulence in the present study. It should be noted that the Rossby deformation radius $L_D(\mu)$ is expressed using Rossby and Froude numbers as

$$L_D(\mu) = \frac{\sqrt{\Phi_0}}{2\Omega|\mu|} = \frac{\mathrm{Ro}}{\mathrm{Fr}}\frac{a}{|\mu|}. \tag{4}$$

To perform numerical experiments, the dependent variables are expanded by spherical harmonics $Y_n^m(\lambda,\mu)$, and the pseudospectral method is adopted to calculate the nonlinear terms in Eqs. (1)-(3). The numerical model resolution is 512×256 grids in the longitudinal and latitudinal directions and the triangular truncation wavenumber is 170, which is determined by the no-aliasing condition in evaluating the nonlinear terms. A fourth-order Runge-Kutta scheme is used for time integration. Although a leapfrog scheme is often adopted in many studies (e.g. Cho and Polvani 1996), it may be disadvantageous for the proper treatment of fast frequency modes like gravity modes. By using the Runge-Kutta scheme, the disadvantages arising in the treatment of gravity waves in time integration schemes can be avoided. Moreover, explicit timestepping is

adopted since implicit timestepping artificially slows down gravity wave speeds and may not preserve wave-mean flow interactions. The order of hyperviscosity and its coefficient are set using values of $p = 4$ and $\nu_{2p} = 3.0 \times 10^{-17}$, respectively.

The initial field is composed of vorticity only, and its power spectrum is assumed to be the same distribution function as that used by Cho and Polvani (1996),

$$E_n(t=0) = \frac{An^{\gamma/2}}{(n+n_0)^{\gamma}}, \quad E_n = \sum_{m=-n}^{n} \frac{|\zeta_n^m|^2}{2n(n+1)}. \tag{5}$$

The phase of each mode is randomly determined. The vorticity skewness in the initial field is not assumed to be exactly zero, but still vanishingly small, and asymmetry between cyclones and anticyclones can be ignored in the initial state. Equation (5) can be regarded as the initial energy spectrum since divergence and geopotential are both zero in the initial state. However, it should be noted that the energy spectrum in the quadratic terms of the expansion coefficients cannot be precisely formulated because the general expression of energy in shallow water is not quadratic (Farge and Sadourny 1989). A constant A is determined so that the initial total energy $E = \sum_{n=2}^{N} E_n$ equals $1/2$ (*i.e.* the representative velocity scale $U_0 = \sqrt{2E}$ is unity). Parameters n_0 and γ characterize the peak wavenumber and width, respectively, in the distribution of the power spectrum and are set to be $\{n_0, \gamma\} = \{40, 40\}$ throughout the experiments. In this study, we examine only the range of parameters for which the scale of the initial vortices is not overly larger than the Rossby deformation radius at the poles, $(\mathrm{Ro}/\mathrm{Fr})a$. The selection of this scale has two meanings. First, the avoidance of gravity wave radiation in the initial geostrophic adjustment is important since the initial field in our experiments is not balanced, unlike the setup by Cho and Polvani (1996). The ratio of gravity modes included in the initial field is less than 2 % in the parameter range we examined, and our preliminary experiments with the initial field satisfying gradient-wind balance indicate that

the initial balance does not have crucial effects on the statistical features seen in the equilibrium state in our parameter range. Second, a jet scale in an equilibrium state may be directly controlled by the scale of initial vortices, if the scale of vortices is much larger than the deformation radius. In shallow-water turbulence, vortices larger than the deformation radius cease to merge (Polvani et al. 1989), and upscale energy cascade is suppressed. The occurrence of an upscale energy cascade is considered to be necessary for investigating the determining factor of the meridional scale of an equatorial jet.

In the standard experiments, we focus on ensemble experiments for Ro $= 0.01$, 0.02 and 0.03, using a fixed Froude number Fr $= 0.3$, where the effects of divergence strongly appears. The number of ensemble members is 125 for Ro $= 0.01$, 0.02 and 1000 for Ro $= 0.03$. Time integrations are halted at $t = 15$, where flow fields are close to an equilibrium state. This parameter range is limited and cannot be applied to the terrestrial atmosphere and gas giants. The purpose of our study is to examine the robustness of the retrograde equatorial jet on shallow-water turbulence rather than to explore a wide parameter range. Time is scaled with $a/U_0 = 1\mathrm{day}/(4\pi\mathrm{Ro})$, which is identical to the scaling in Cho and Polvani (1996), so that $t = 15$ corresponds to 119 planetary rotations for $\mathrm{Ro} = 0.01$ and 39.8 for $\mathrm{Ro} = 0.03$.

2b. *Results*

[Figure 1 about here.]

Figure 1 shows histograms of a zonal-mean zonal flow at the equator at $t = 5$ and 15. The distribution of the histogram is almost symmetric at $t = 5$ and the variance of the histogram is similar among the parameter sets examined in our experiments. This implies that an equatorial flow formed by an initial mixing process is not biased in the direction of the equatorial zonal

flow and is strongly dependent on the initial distribution of vortices rather than on nondimensional parameters. On the other hand, the distribution of the histogram shifts to the negative (retrograde) side with time, and this tendency is more pronounced for smaller Rossby numbers. In particular, an equatorial flow is retrograde in all the cases for $\mathrm{Ro} = 0.01$. This result is consistent with Cho and Polvani (1996). However, an equatorial prograde flow dependent on the initial field can also exist for $\mathrm{Ro} = 0.02$ and 0.03, and the probability of emergence of the prograde flow increases with increasing Rossby number. It should be noted that the number of the members, where $\langle u \rangle$ ($\langle \cdot \rangle$ denotes longitudinal average) is over 0.5, increases with elapsed time in evolution for $\mathrm{Ro} = 0.03$. This result suggests the existence of acceleration of a prograde flow as well as a retrograde one.

[Figure 2 about here.]

In order to verify the persistence of the equatorial prograde flow appearing for $\mathrm{Ro} = 0.03$, time integration is performed until $t = 50$ for 50 ensemble members for which prograde flow has been confirmed. Figure 2 shows histograms of the equatorial zonal flow with these ensemble members at $t = 15$ and 50. Although the distribution of the histogram broadens with time, and the number of prograde jets decreases between $t = 15$ and $t = 50$, there are ensemble members for which a prograde flow remains. This result suggests that an equatorial prograde flow can spontaneously emerge and remain without experiencing decrease in its velocity even after sufficiently long time integration.

[Figure 3 about here.]

As the zonal-mean zonal flow is evaluated at only one latitudinal point in Fig. 1, it is necessary to confirm whether the equatorial zonal flow has a jet shape which characteristically appears as a zonally elongated rapid flow concentrated in a narrow region. The zonal-mean zonal flow, vorticity,

and geopotential anomaly at $t = 15$ are shown for the ensemble member producing the strongest flow at the equator in Fig. 3. A remarkable jet shape is seen in both retrograde and prograde cases. In particular, the predominance of a prograde jet seen in Fig. 3(b) has not been observed in previous studies and its presence indicates that the conclusion presented in Cho and Polvani (1996), that the direction of the equatorial jet is always retrograde, does not exactly apply for our parameter range. However, the probability for the emergence of a prograde jet is small, as is shown in Fig. 1. We calculate an asymmetry index introduced by Iacono et al. (1999) in order to examine the relationship between an equatorial zonal flow and vorticity skewness. Figure 4 presents the time evolution of the asymmetry index and the zonal flow at the equator for the case shown in Fig. 3(b). Although the equatorial flow is always prograde, the sign of the asymmetry index changes at $t \sim 40$. This may be due to the fact that vorticity skewness is largely dependent on the asymmetry of coherent vortices appearing at high latitudes, while the magnitude of the equatorial flow is determined by the vorticity within the jet region. This simple example suggests that vorticity skewness evaluated over the sphere is not useful in making an analysis on the magnitude of an equatorial jet.

[Figure 4 about here.]

Potential vorticity (PV) fields, which correspond to retrograde and prograde jets, are shown in Fig. 5. While coherent vortices are found at mid- and high latitudes, a dominant zonal structure is present in the equatorial region where a jet appears, and PV mixing on either side of the prograde jet and homogenization thoroughly occur. However, there is a difference in the latitudinal distribution of PV between the retrograde and prograde cases. When a retrograde jet emerges, positive and negative PV anomalies appear in the northern and southern regions of the equator, respectively, and PV homogenization occurs across the equator. On the other hand, in the prograde case, the

PV anomaly is positive (negative) in the northern (southern) region, and PV gradient increases at the equator. Namely, the direction of the equatorial jet corresponds to the distribution of the region where PV homogenization in retrograde regions occurs.

[Figure 5 about here.]

Returning to Fig. 3, we may note the width of the equatorial jet. The meridional profile of the zonally-uniform (the zonal wavenumber m is zero) Rossby mode with the lowest meridional wavenumber ($l = 1$) is drawn in Fig. 3 for comparison, but the geopotential anomaly is derived from the gradient wind balance to satisfy the steady state in Eqs. (1)–(3). Here, the structure of each of the zonally-uniform Rossby modes is defined as the eigenmode in the $m \to 0$ limit, since the eigenmodes of the shallow-water equations (the Hough modes) have the degenerate zero frequency modes for $m = 0$. This treatment is reasonable because it has been proven that the eigenmodes calculated in such a way are consistent with the structure of the Rossby and Kelvin modes for $m \neq 0$ (Shigehisa 1983). The zonal-mean flow structure and the width of the equatorial jet coincide well with those of the Rossby mode having the lowest meridional wavenumber. This result suggests that the width of the equatorial jet can be characterized by the Rossby deformation radius at the equator $L_{D(\mathrm{eq.})} \equiv (\sqrt{\Phi_0}/\beta)^{1/2}$, since the meridional structures of the equatorial waves are determined by $L_{D(\mathrm{eq.})}$ (Matsuno 1966).

If the scale of the jet is determined by $L_{D(\mathrm{eq.})}$, as is seen in Fig. 3, we can estimate the upper limit of the jet magnitude with the Rossby mode for $l = 1, m \to 0$. We assume that the upper limit of the jet magnitude is determined by the largest magnitude of the Rossby mode such that there is no negative PV gradient region, since a negative PV gradient state cannot be maintained due to barotropic instability. Under this assumption, we obtain the range of the possible jet magnitude as $-1.45 < \langle u \rangle < 1.72$ for $\{\mathrm{Ro}, \mathrm{Fr}\} = \{0.01, 0.3\}$ and $-1.49 < \langle u \rangle < 1.70$ for $\{\mathrm{Ro}, \mathrm{Fr}\} =$

$\{0.03, 0.3\}$. The magnitude of the equatorial zonal flow is within this range for all the ensemble members (Fig. 1).

3. Acceleration of a jet induced by waves

3a. *Objectives*

In the previous section, we have seen that both the retrograde and prograde equatorial jets can be spontaneously dominant in shallow-water turbulence. The principal purpose of this section is to examine the acceleration mechanisms of the equatorial jet. Two kinds of mechanisms for zonal-mean flow acceleration are commonly proposed: (i) PV mixing and homogenization due to turbulent motion and (ii) wave-wave interactions. In the section below, we will discuss the role of each mechanism in equatorial jet formation independently, although both mechanisms can coexist in rotating shallow-water.

The concept of the zonal flow formation due to PV homogenization is applied to many problems (Rhines 1977; Rhines and Holland 1979; McIntyre 1982; Rhines 1994). In the barotropic case, PV homogenization process is more predominant in the higher latitude, where the effect of the linear process is smaller due to the larger Rhines scale. On the other hand, for the $L_D/a \ll 1$ case treated in our experiments, this concept can be applied to shallow-water turbulence in the following manner. While coherent vortices hardly interact and turbulent mixing is inactive in the mid- and high latitudes because of the small deformation radius, PV homogenization is more active in the equatorial region where the deformation radius is larger compared to high latitudes where the Rhines scale is larger. We can speculate two configurations for PV homogenization in the equatorial region (Fig. 6). While the occurrence of PV homogenization across the equator corresponds to

a retrograde jet, a PV edge at the equator yields a prograde one. The PV inversion procedure, when a gradient wind balance is assumed, gives the meridional profile of the zonal flow as the steady state. The zonal-mean PV distribution tends to have a uniform zone with sharp gradients at the south and north edges only in the equatorial region. On the other hand, if initial mixing makes a prograde flow, PV gradient is greater on the equator and smaller in a strip off the equator. In such cases, it is expected that PV homogenization should be facilitated in the strip off the equator. The configuration realized depends on the initial condition. As the PV gradient increases, the restoring force in the meridional direction is intensified and nonlinear advection is relatively suppressed. As a result, the PV edge forms a barrier against a Lagrangian motion across the edge, and the equatorial jet can be sustained without meridional momentum transfer by waves.

[Figure 6 about here.]

This idea surely elucidates that a equatorial jet profile is sustained in cases where a strong jet appears, and the relationship between the zonal velocity and the PV is consistent with the results of the previous section (Fig. 3, 5). However, it appears to be insufficient for understanding the *statistical* distribution of the equatorial jet magnitude (Fig. 1). While the above argument suggests that the collapse of a uniform PV zone and its edges formed in the initial stage would not occur from subsequent PV homogenization process, the histogram shown in Fig. 1 shifts wholly in the retrograde direction, even when a prograde flow is formed in the initial stage. To understand the statistical distribution of the equatorial flow, we should also explore the other candidate for the jet acceleration mechanism; the zonal-mean flow acceleration induced by wave-wave interactions.

The acceleration mechanism by waves is based on the conservation law of pseudo-angular momentum. When pseudo-angular momentum of a wave is lost, it gives rise to zonal flow acceleration. Hayashi et al. (2000) applied this theory to 2D nondivergent turbulence and examined

whether retrograde acceleration in a polar jet induced by waves is consistent with that of a weak-nonlinear model. A similar approach in a shallow-water system on the spherical geometry was also taken to investigate zonal-mean flow acceleration due to shear instability (Iga and Matsuda 2005). According to their formulation, we examine the acceleration of a zonal flow in shallow-water turbulence using a weak nonlinear model.

3b. *Model description*

To construct a set of weak nonlinear equations, the dependent variables are expanded around a zonally uniform basic flow following Hayashi et al. (2000). We suppose that the deviation field can be expanded into a series of amplitudes with a small parameter $\epsilon \ll 1$, as:

$$\begin{aligned}
\zeta &= \zeta_0(\mu) + \epsilon\zeta_1(\lambda,\mu,t) + \epsilon^2\zeta_2(\mu,t) + O(\epsilon^3), \\
D &= \epsilon D_1(\lambda,\mu,t) + \epsilon^2 D_2(\mu,t) + O(\epsilon^3), \\
\Phi &= \Phi_0(\mu) + \epsilon\Phi_1(\lambda,\mu,t) + \epsilon^2\Phi_2(\mu,t) + O(\epsilon^3).
\end{aligned}$$

Here, the subscript represents the order of magnitude of disturbance. The zeroth order of the variables represents a given basic state and the second order is assumed to be zonally uniform. It should be noted that there is no zeroth divergence term, because the divergent component in a steady state vanishes in the shallow-water equations. If the equations are satisfied for an arbitrary small parameter ϵ, the deviation field must balance in each power of ϵ. Substituting the above into the shallow-water equation (1)–(3) and the same order collection with respect to ϵ yields the

first-order linear equations,

$$\frac{\partial \zeta_1}{\partial t} = -\frac{1}{1-\mu^2}\left[\frac{\partial}{\partial \lambda}\left\{(f+\zeta_0)\,U_1+\zeta_1 U_0\right\}+(1-\mu^2)\frac{\partial}{\partial \mu}\left\{(f+\zeta_0)\,V_1\right\}\right]+d_{\zeta_1}, \quad (6)$$

$$\frac{\partial D_1}{\partial t} = \frac{1}{1-\mu^2}\left[\frac{\partial}{\partial \lambda}\left\{(f+\zeta_0)\,V_1\right\}-(1-\mu^2)\frac{\partial}{\partial \mu}\left\{(f+\zeta_0)\,U_1+\zeta_1 U_0\right\}\right] -\Delta\left(\frac{\Phi_1}{\mathrm{Fr}^2}+\frac{U_0 U_1}{1-\mu^2}\right)+d_{D_1}, \quad (7)$$

$$\frac{\partial \Phi_1}{\partial t} = -\frac{1}{1-\mu^2}\left[\frac{\partial}{\partial \lambda}\left(U_0\Phi_1+U_1\Phi_0\right)+(1-\mu^2)\frac{\partial}{\partial \mu}\left(V_1\Phi_0\right)\right]-D_1+d_{\Phi_1}, \quad (8)$$

and the second-order equations,

$$\frac{\partial \zeta_2}{\partial t} = -\frac{\partial}{\partial \mu}\left[(f+\zeta_0)\,V_2+\langle \zeta_1 V_1\rangle\right], \quad (9)$$

$$\frac{\partial D_2}{\partial t} = -\frac{\partial}{\partial \mu}\left[(f+\zeta_0)\,U_2+\langle \zeta_1 U_1\rangle+\zeta_2 U_0\right]-\Delta\left(\frac{\Phi_2}{\mathrm{Fr}^2}+\frac{\langle U_1^2+V_1^2\rangle+U_0U_2}{2(1-\mu^2)}\right), \quad (10)$$

$$\frac{\partial \Phi_2}{\partial t} = -\frac{\partial}{\partial \mu}\left(\langle V_1\Phi_1\rangle+V_2\Phi_0\right)-D_2. \quad (11)$$

Here, the term d_{ζ_1,D_1,Φ_1} represents the effect of wave dissipation, which gives rise to the second-order acceleration in respect to the small parameter ϵ. In these experiments, the same dissipation form as the full nonlinear model is assumed. It should be noted that Hayashi et al. (2000) assumed that the second-order acceleration is replaced by the acceleration of the basic field in their formulation (the LHS terms in (9)–(11) are replaced by time deviation of the zeroth-order variables). Since we do not adopt their assumption, the waves represented by the first order are not modified by the second-order variables.

In the present experiments, Eqs. (6)–(11) are integrated from the initial field which is identical to the eddy field (removing zonal-mean components) at $t = 5$ calculated by the full nonlinear model described in the previous section. We use three datasets for the initial field:

1. 125 members, which are identical to those used in the full nonlinear experiments for $\mathrm{Ro} = 0.01, \mathrm{Fr} = 0.3$.

2. 50 members where a prograde jet appears in the nonlinear experiments for $\mathrm{Ro} = 0.03, \mathrm{Fr} = 0.3$ (hereafter referred to as a prograde dataset).

3. 50 members where a retrograde jet appears in the nonlinear experiments for $\mathrm{Ro} = 0.03, \mathrm{Fr} = 0.3$ (a retrograde dataset).

For each dataset, we examine three types of basic fields: no basic flow, a prograde equatorial jet, and a retrograde equatorial jet. The zonal flow profile of the basic field is assumed to be the vorticity field of the Rossby mode with $l = 1, m = 0$, and the geopotential field is determined by gradient wind balance so that the given basic field is steady. It can be seen from the previous section that this profile is a reasonable idealization. The magnitude of the equatorial jet peak is set to be 0.5 throughout the experiments.

All wave components can be decomposed into Rossby and gravity modes based on the Hough mode expansion, and contributions to the second order acceleration can be divided into two parts; one is from the products of two-Rossby modes, the other from the products of two gravity modes or those of one-Rossby and one-gravity modes. For simplicity, all westward-propagating mixed Rossby-gravity (MRG) modes are categorized into Rossby modes.

3c. *Results*

[Figure 7 about here.]

First, acceleration of the zonal flow due to wave-wave interactions without a basic flow is examined, and results are presented in Fig. 7. In the left panels, acceleration defined as $\langle u(t =$

$15)\rangle - \langle u(t=5)\rangle$ obtained from the full nonlinear experiments is shown for comparison. Acceleration in the full nonlinear experiments concentrates in the equatorial region and its variance is small. In the prograde cases, zonal flow acceleration intensifying a prograde flow occurs, but it is much smaller than that seen in the retrograde cases. This implies that the acceleration mechanism in the prograde direction certainly exists, but that its effects are much smaller compared to the acceleration in the retrograde direction. In all of the weak nonlinear experiments, the Rossby modes are almost the sole contributing factor to second-order acceleration, and contribution from the gravity modes can be ignored. For $\mathrm{Ro} = 0.01$, acceleration in the retrograde direction is clearly seen in the weak nonlinear experiment as well as the full nonlinear one and is quantitatively consistent. On the other hand, zonal flow acceleration induced by waves is weak and always retrograde for $\mathrm{Ro} = 0.03$. There is little difference between the prograde and retrograde datasets. Namely, the results show that the direction of zonal flow acceleration in the weak nonlinear framework is independent of the initial configuration of eddies. This second-order acceleration is clearly inconsistent in the prograde dataset and much weaker than the acceleration obtained in the full nonlinear experiments, even for the retrograde ones. Regardless of which dataset is used, these results cannot explain the acceleration of the equatorial jet obtained in the full nonlinear experiments for $\mathrm{Ro} = 0.03$. It should be noted that the variance in the mid-latitudes is large due to the dispersion of coherent vortices, which exist stably in the full nonlinear model, giving rise to artificial transport of pseudo-angular momentum in the weak nonlinear model. For this reason, the results in the mid- and high-latitudes have low reliability.

[Figure 8 about here.]

Second, the results with a basic flow are shown in Fig. 8. Although deformation of an initial Rossby wave due to the basic flow may generate a gravity wave and *vice versa*, it must be pointed

out that our decomposition of contribution to the second-order acceleration does not take this effect into account. Since the Hough mode decomposition is performed in the initial state only, contribution from gravity modes generated during time evolution is also included in the left panels of Fig. 8.

For $\mathrm{Ro} = 0.01$, the second-order acceleration is always retrograde and has two peaks. These features are especially remarkable in the experiment with a retrograde jet. As will be discussed in the next subsection, these accelerations may be regarded as the result of the absorption of Rossby waves at critical latitudes. It should be noted that such a zonal-mean flow profile cannot be realized in the nonlinear framework, since barotropic instability occurs and deforms the zonal-mean flows, resulting in decreased latitudinal shear. The results for $\mathrm{Ro} = 0.03$ are quite different from those for $\mathrm{Ro} = 0.01$. The second-order acceleration works as a positive feedback for the given basic flow at the equator. This tendency is similar to that seen for the retrograde dataset (not shown). Namely, it is the basic flow profile rather than the eddies in the initial state which control the direction of acceleration at the equator. These results suggest that both directions of the equatorial jet can be intensified and sustained, as opposed to the $\mathrm{Ro} = 0.01$ cases, if there is an equatorial jet in the initial state.

[Figure 9 about here.]

Furthermore, we have extracted westward propagating MRG waves only from the initial disturbance at $t = 5$ to examine the acceleration induced by these waves for $\mathrm{Ro} = 0.03$. It can be seen from Fig. 9 that these waves generate acceleration which intensifies the basic flow, and that their contribution accounts for approximately half of the total acceleration when compared to the results in Fig. 8. It seems that the deformation of MRG waves by the zonal flow plays an important role in the intensification mechanism of the equatorial jet.

3d. *Acceleration mechanisms of an equatorial jet*

Here, we will discuss the acceleration mechanisms of an equatorial jet emerging in shallow-water turbulence in terms of the weak nonlinear framework. Following the results of the previous subsection, we will mainly focus on the contributions of the Rossby and MRG waves.

The first mechanism is involved with acceleration to the retrograde direction, which is the prominent feature of the $\mathrm{Ro} = 0.01$ cases. As is discussed in Hayashi et al. (2000), absorption of Rossby waves at the equator is expected to induce retrograde acceleration of an equatorial flow, since the pseudo-angular momentum of Rossby waves is always negative (Hayashi and Young 1987; Iga and Matsuda 2005). By adopting the WKBJ approximation for a shallow-water system on a β plane for simplicity, we obtain the phase velocity for a Rossby wave packet as follows:

$$c = \langle u \rangle - \frac{\tilde{\beta}}{k^2 + l^2 + 1/L_D^2}, \quad \tilde{\beta} = \beta - \langle u \rangle_{yy} + \frac{f \langle h \rangle_y}{H + \langle h \rangle}, \tag{12}$$

where the subscript y denotes differentiation in the meridional direction. While the longitudinal wavenumber k and the phase velocity c are conserved along a ray, the meridional wavenumber l is variable as

$$l^2 = -(k^2 + 1/L_D^2) + \frac{\tilde{\beta}}{\langle u \rangle - c}, \tag{13}$$

so that the dispersion relation (12) is satisfied. The meridional wavenumber l becomes larger with increasing deformation radius L_D or when the phase velocity approaches the zonal velocity. Then, a Rossby wave with a large l tends to dissipate and lose its pseudo-angular momentum. Although the energy dissipation rates of Rossby waves depend on the order of the hyperviscosity operator and value of the coefficient, the qualitative behavior of pseudo-angular momentum transfer due to the waves is independent of them. We will examine how a meridional wavenumber of a Rossby wave

packet propagating from $\mu = \mu_0$ to $\mu = \mu_1$ ($|\mu_0| > |\mu_1|$) varies. If there is no basic flow on the β plane, the meridional wavenumber satisfies the relationship $l_1^2 = l_0^2 + (\mu_0^2 - \mu_1^2)\mathrm{Fr}^2/\mathrm{Ro}^2$, where l_0 and l_1 are the meridional wavenumbers at $\mu = \mu_0$ and $\mu = \mu_1$, respectively. This relationship suggests that l_1 becomes remarkably larger even for the same initial wavenumber l_0, when the Rossby number is smaller. Therefore, increase in the meridional wavenumber by variation of L_D with respect to latitude induces retrograde acceleration through wave dissipation for small Rossby numbers, even when there is no basic flow. On the other hand, treatment of the latter condition, that the phase velocity is close to the zonal velocity, is slightly more complicated. We will suppose that a Rossby wave packet is initially located outside the equatorial jet region so that its phase velocity is not affected by the basic flow. The phase velocity of the wave packet can be approximately expressed in the nondimensional form as:

$$c_0 \sim -\frac{\frac{\cos\theta_0}{\mathrm{Ro}}}{K^2 + \left(\frac{\mathrm{Fr}}{\mathrm{Ro}}\right)^2 \sin^2\theta_0}, \tag{14}$$

where θ_0 is the latitude of the initial position of the wave packet and $K^2 = k^2 + l^2$. Since the initial phase velocity c_0 is conserved along the ray, the condition that a critical latitude exists for the Rossby wave packet propagating to the equatorial jet region can be simply described as $\min(u_0) < c_0 < 0$. The phase velocity for the small wavenumber region is important for considering whether the wave absorption at the critical latitude also works in the full-nonlinear experiment, because motions having scales larger than the deformation radius can behave as a wave in the full nonlinear framework. Therefore, we now focus on long waves whose wavenumbers satisfy the inequality $K^2 < (\mathrm{Fr}/\mathrm{Ro})^2 \sin^2\theta_0$. The dominant part of Eq. (14) for the small wavenumbers can be written

as:

$$c_0 \sim -\frac{\mathrm{Ro}\cos\theta_0}{\mathrm{Fr}^2\sin^2\theta_0}. \tag{15}$$

Equation (15) indicates that the phase velocity at a given latitude is slower and the criterion for a Rossby wave to have a critical latitude is easily satisfied since the Rossby number is smaller. In both cases, retrograde acceleration due to the absorption of a Rossby wave propagating toward the equator works well when the Rossby number is small, and this conclusion is consistent with the result of our experiments.

[Figure 10 about here.]

On the other hand, MRG waves seem to offer a clue to another mechanism for intensifying a basic flow. When there is an equatorial jet in a basic flow, equatorial waves may be modified by equatorial jet shear. If the structures of the equatorial waves are nearly geostrophic like the one shown in Fig. 10, the modified waves can have correlation between u_1 and v_1, which involves meridional transfer of pseudo-angular momentum. This momentum transfer is expected to intensify the basic flow. Westward-propagating MRG waves become close to achieving geostrophic balance when these zonal scales are smaller than the deformation radius at the equator.

[Figure 11 about here.]

In order to investigate the validity of this scenario, we will examine the acceleration due to a monochromatic MRG wave using the weak nonlinear model having a basic flow. In this experiment, the representative velocity of an initial wave is unity. Figure 11 shows the second-order zonal flow induced by an MRG wave at $t = 1$ for $\mathrm{Ro} = 0.03$. In this figure, a negative m represents a westward-propagating mode. As for the westward-propagating MRG wave, acceleration intensifying the basic flow becomes stronger at shorter zonal wavelength, as is expected. Although

an MRG wave with a long wavelength induces second-order flow and thereby weakens the basic flow, it is not steady and its amplitude is negligible. An eastward-propagating wave does not contribute to acceleration at all. Furthermore, similar experiments for Kelvin and Rossby waves with the lowest meridional wavenumber were performed, and the results are shown in Fig. 12. The second-order acceleration induced by the Rossby wave has a double-peak structure, and its value at the equator is zero. Acceleration due to a Rossby wave having higher meridional wavenumbers would have more peaks. The Kelvin wave does not contribute to zonal flow acceleration. Only MRG waves having a negative m induce acceleration with a single peak at the equator.

[Figure 12 about here.]

This simple examination indicates that the scenario mentioned above is valid. The reason why this mechanism does not work sufficiently for $\mathrm{Ro} = 0.01$ may lie in the smaller deformation radius. While a longitudinal scale of an MRG wave smaller than the equatorial deformation radius is necessary in order to satisfy the geostrophic balance, as shown in Fig. 10, the power spectrum in the turbulent field decreases with the zonal wavenumber. Hence, acceleration due to an equatorial wave tilting is weaker at smaller deformation radii.

4. Concluding remarks

In order to confirm the robustness of the equatorial retrograde jet emergence in shallow-water turbulence reported by Cho and Polvani (1996), ensemble experiments with various initial states were performed, and the dependencies of the direction and magnitude of the equatorial jet on the initial state were investigated using the statistical distributions of zonal flows at the equator. For a given $\mathrm{Fr} = 0.3$, the histogram for magnitude of the equatorial flow shifts in the retrograde direction

with time. While a prograde jet at the equator does not appear for the small Rossby number cases, both a steady prograde equatorial jet and a retrograde jet can exist for large Rossby numbers. In this sense, the conclusion reached by Cho and Polvani (1996) that a prograde equatorial jet is not possible is not precise.

Furthermore, we examined the second-order acceleration induced by wave-wave interactions with the weak nonlinear model. The results obtained from the weak nonlinear experiments were qualitatively consistent with those of the full nonlinear ones, and it has been shown that analysis based on the weak nonlinear framework is useful for exploring the acceleration mechanisms of the equatorial jet emerging in shallow-water turbulence. Based on the results of the weak nonlinear experiments, the mechanisms for second-order acceleration by waves could be categorized into two types. The first mechanism is related to the increase of the local meridional wavenumber of Rossby waves propagating to the equator. Dissipation of a Rossby wave, whose pseudo-angular momentum is negative, always induces zonal flow acceleration in the retrograde direction, and this mechanism seems to have more pronounced effects at smaller Rossby numbers. In the second mechanism, the westward-propagating MRG waves tilted by meridional shear of the zonal-mean flow transfer the pseudo-angular momentum. A basic equatorial flow is intensified by the mechanism, and it works efficiently for the larger Rossby deformation radius at the equator. However, an equatorial jet must be formed in the initial stages in order for the second acceleration mechanism to take effect.

The equatorial jet formation in the parameter range examined in our study can be summarized as follows. A retrograde jet can be generated by transfer of pseudo-angular momentum due to a Rossby wave packet propagating to the equatorial region, regardless of whether or not there is a jet formation process resulting from PV mixing due to turbulent motion. On the other hand, increase

of PV gradient at the equator due to PV mixing in the initial stage is necessary for the development of a prograde jet, regardless of which mechanism plays the major role in the formation process, the PV homogenization or wave-wave interactions. In particular, prograde acceleration does not occur spontaneously in the weak nonlinear framework. While the histogram at $t = 5$ shown in Fig. 1 suggests that the formation of the equatorial flow in the initial stage is strongly dependent on the initial distribution of vortices, an in-depth analysis on jet formation due to initial mixing of vortices is beyond the scope of the present study, although it is important for understanding the conditions necessary for prograde jet formation. Further studies are necessary to make a more comprehensive study on the factors determining the direction of the equatorial jet in shallow-water turbulence.

Acknowledgement One of the authors (Y. K.) is supported by the JSPS Research Fellowships. All figures have been drawn using the GFD-DENNOU Library (SGKS Group 1995).

References

Charney, J. G., 1971: Geostrophic turbulence. *J. Atmos. Sci.*, **28**, 1087–1095.

Cho, J. Y.-K. and L. M. Polvani, 1996: The emergence of jets and vortices in freely evolving, shallow-water turbulence on a sphere. *Phys. Fluids*, **8**, 1531–1552.

Farge, M. and R. Sadourny, 1989: Wave-vortex dynamics in rotating shallow water. *J. Fluid Mech.*, **206**, 433–462.

Hayashi, Y.-Y., K. Ishioka, M. Yamada, and S. Yoden, 2000: Emergence of circumpolar vortex in 2-D turbulence on a rotating sphere. *IUTAM Symposium on Developments in Geophysical*

Turbulence (Proceedings of the IUTAM Symposium held at the National Center for Atmospheric Research, Boulder, CO, 16-19 June 1998, Kluwer Academic Publishers, 179–192.

Hayashi, Y.-Y. and W. R. Young, 1987: Stable and unstable shear modes of rotating parallel flows in shallow water. *J. Fluids Mech.*, **184**, 477–504.

Huang, H.-P., B. Galperin, and S. Sukoriansky, 2001: Anisotropic spectra in two-dimensional turbulence on the surface of a rotating sphere. *Phys. Fluids*, **13**, 225–240.

Iacono, R., M. V. Struglia, and C. Ronchi, 1999: Spontaneous formation of equatorial jets in freely decaying shallow water turbulence. *Phys. Fluid*, **11**, 1272–1274.

Iga, S. and Y. Matsuda, 2005: Shear instability in a shallow water model with implications for the venus atmosphere. *J. Atmos. Sci.*, **62**, 2514–2527.

Lilly, D. K., 1969: Numerical simulation of two-dimensional turbulence. *Phys. Fluids*, **12(Suppl. II)**, 240–249.

Matsuno, T., 1966: Quasi-geostrophic motions in the equatorial area. *J. Meteor. Soc. Japan*, **44**, 25–42.

McIntyre, E., M., 1982: How well do we understand the dynamics of stratospheric warmings? *J. Meteor. Soc. Japan*, **60**, 37–65.

McWilliams, C., J., 1984: The emergence of isolated coherent vortices in turbulent flow. *J. Fluid Mech.*, **146**, 21–43.

Nozawa, T. and S. Yoden, 1997: Spectral anisotropy in forced two-dimensional turbulence on a rotating sphere. *Phys. Fluids*, **9**, 3834–3842.

Polvani, L. M., N. J. Zabusky, and G. R. Flierl, 1989: Two-layer geostrophic vortex dynamics. Part I. upper layer V-state and merger. *J. Fluid. Mech.*, **205**, 215–242.

Rhines, P. B., 1975: Waves and turbulence on a beta-plane. *J. Fluid. Mech.*, **69**, 417–443.

— 1977: The dynamics of unsteady currents. *The Sea, edited by E. D. Goldberg, Vol. VI*, Wiley, New York, 189–318.

— 1994: Jets. *Chaos*, **4**, 313–339.

Rhines, P. B. and W. R. Holland, 1979: A theoretical disbussion of eddy-driven mean flows. *Dyn. Atmos. Ocean*, **3**, 289–325.

Shigehisa, Y., 1983: Normal modes of the shallow-water equations for zonal wavenumber zero. *J. Met. Soc. Japan*, **61**, 479–494.

Vallis, G. P. and M. E. Maltrud, 1993: Generation of mean flows and jets on a beta plane and over topography. *J. Phys. Oceanogr.*, **23**, 1346–1362.

Williams, G. P., 1978: Planetary circulations: 1. barotropic representation of jovian and terrestrial turbulence. *J. Atmos. Sci.*, **35**, 1399–1426.

Yoden, S. and M. Yamada, 1993: A numerical experiment on two-dimensional decaying turbulence on a rotating sphere. *J. Atmos. Sci.*, **50**, 631–643.

Yuan, L. and K. Hamilton, 1994: Equilibrium dynamics in a forced-dissipative f-plane shallow-water system. *J. Fluid Mech.*, **280**, 369–394.

List of Figures

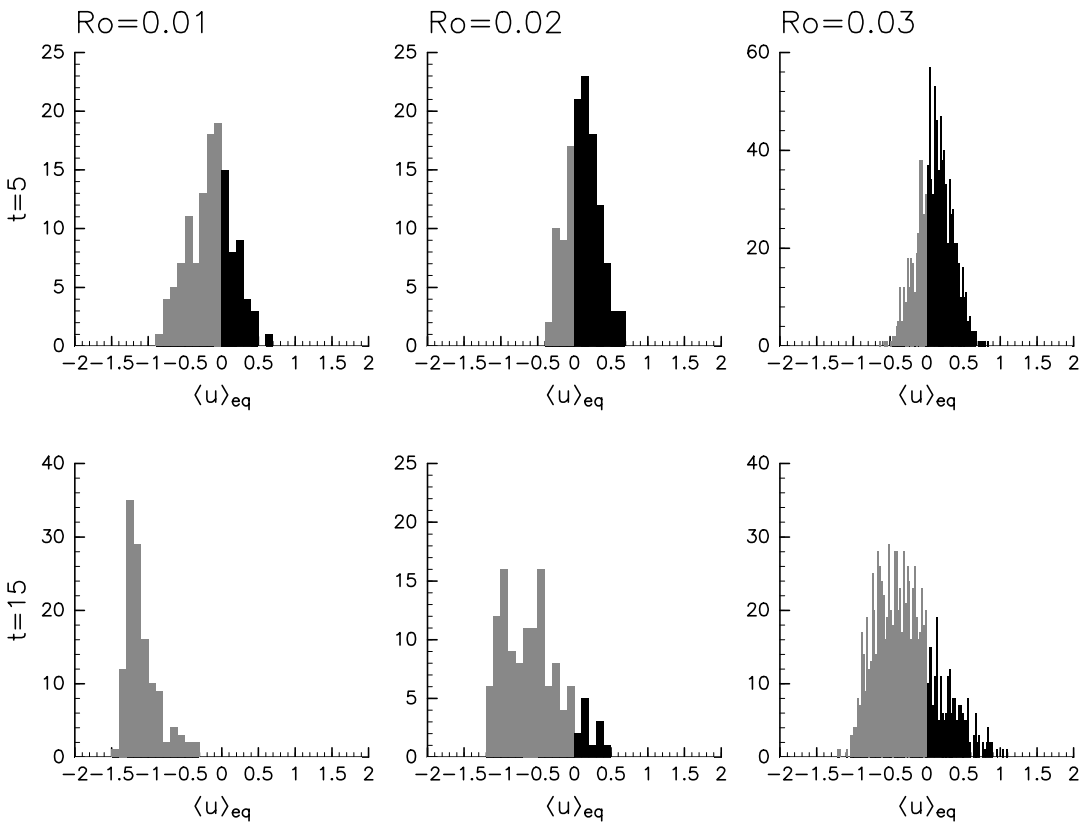

Figure 1: Histogram of the zonal-mean zonal flow at the equator. The left, middle and right panels indicate $\mathrm{Ro} = 0.01$, 0.02, and 0.03 ($\mathrm{Fr} = 0.3$) cases, respectively. The upper and lower panels show the snapshots at $t = 5$ and 15.

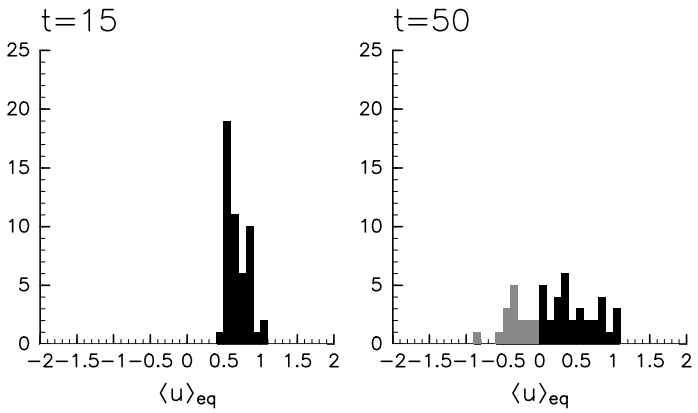

Figure 2: Histograms of an equatorial zonal flow with 50 ensemble members for which a prograde flow at $t = 15$ is confirmed for $\mathrm{Ro} = 0.03$. Left and right panels show snapshots at $t = 15$ and 50.

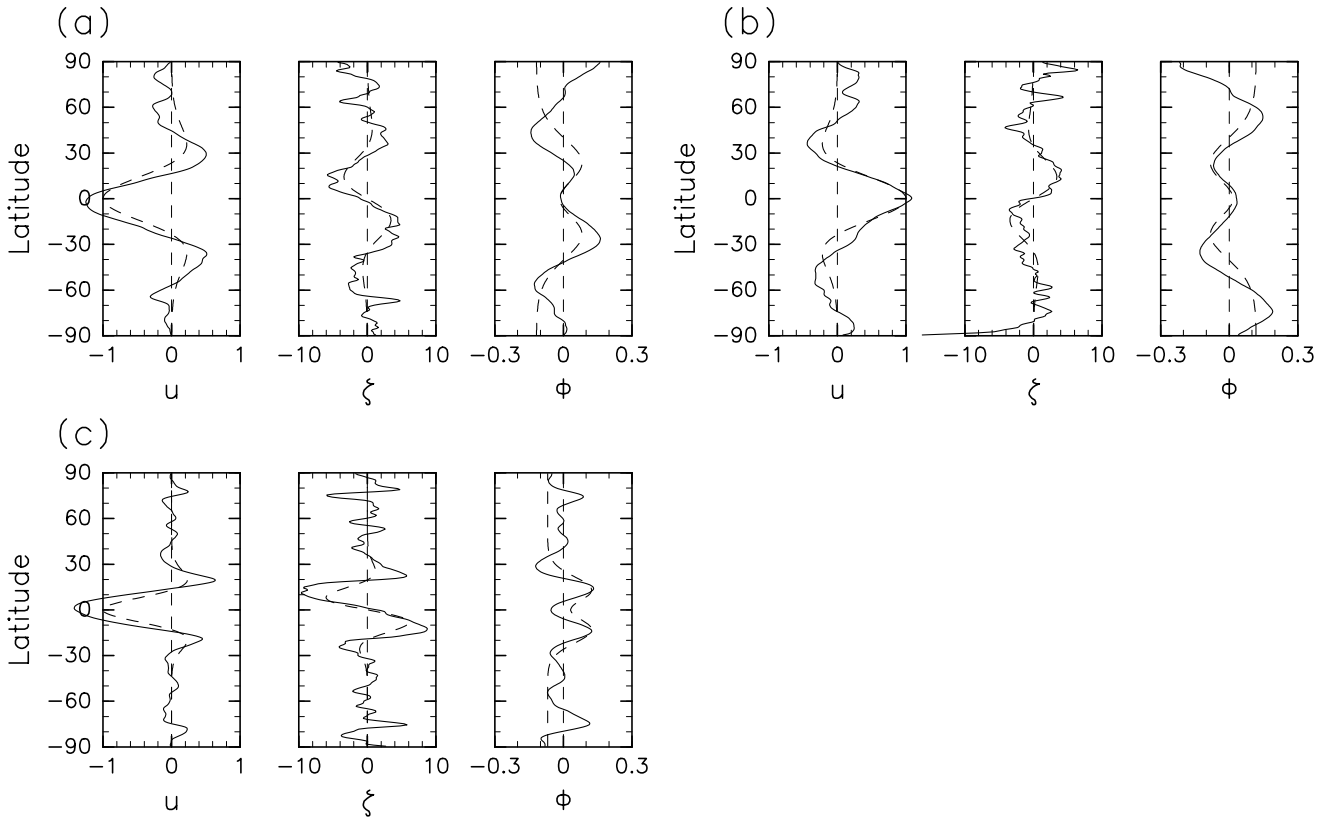

Figure 3: Snapshots at $t = 15$ of the zonal-mean field for the cases where a remarkable jet appears: (a) a retrograde case for $\mathrm{Ro} = 0.03$, (b) a prograde case for $\mathrm{Ro} = 0.03$, and (c) a retrograde case for $\mathrm{Ro} = 0.01$. The dashed line indicates the zonally-uniform Rossby mode with the lowest meridional wavenumber.

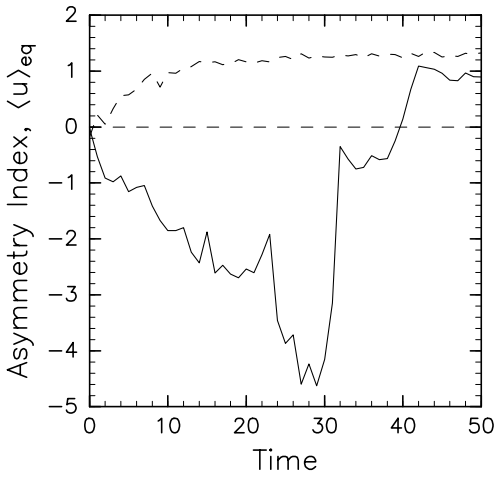

Figure 4: Time evolution of the asymmetric index (solid line) and the zonal-mean zonal flow at the equator (dashed line) for the case shown in Fig. 3(b).

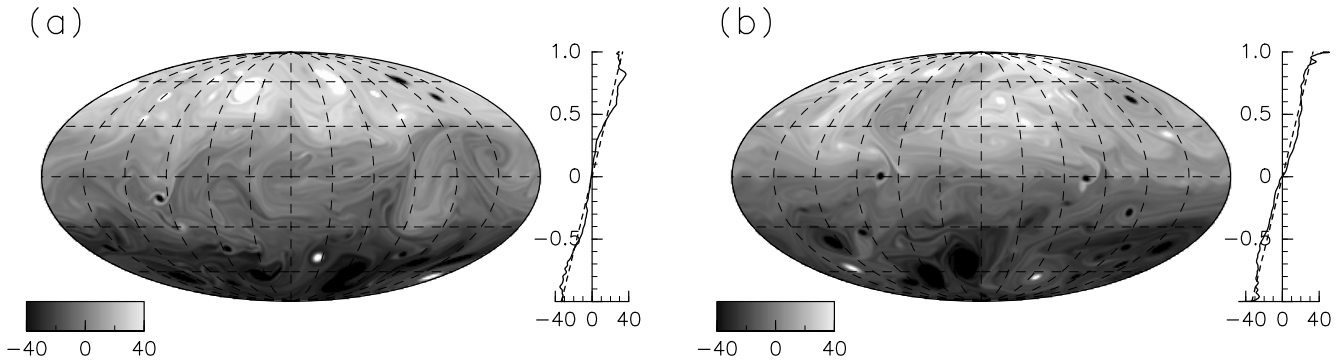

Figure 5: Snapshots at $t = 15$ of potential vorticity field in the cases for (a) a retrograde jet and (b) a prograde jet for $\mathrm{Ro} = 0.03$, $\mathrm{Fr} = 0.3$ in the Mollweide projection. The ensemble members in (a) and (b) are the same as those in Fig. 3. The solid and dashed lines in the right side indicate the zonal-mean of total PV and PV in the state of rest as a function of sine latitude. The vertical and horizontal axes are the sine latitude and the zonal-mean of total PV, respectively.

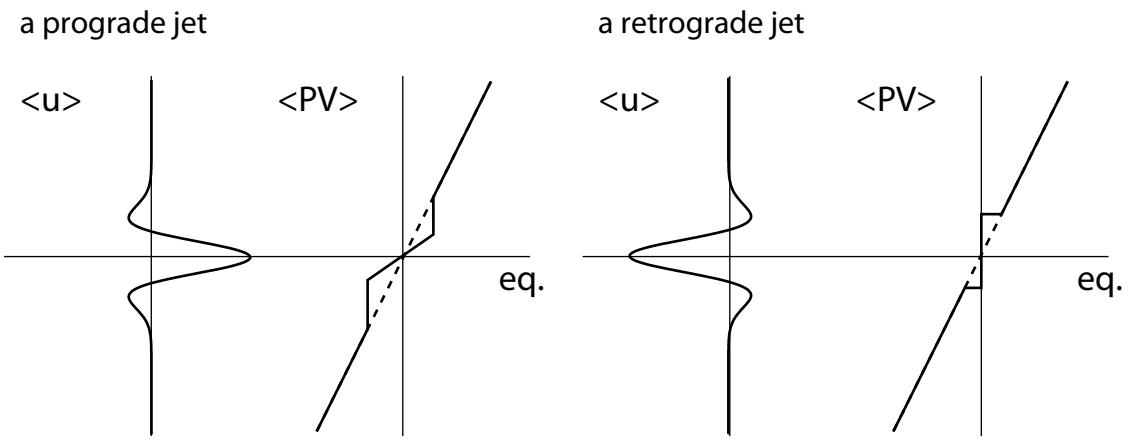

Figure 6: Schematic illustrations for the meridional distribution of the zonal flow and PV. The dashed line represents the PV distribution in the state of rest.

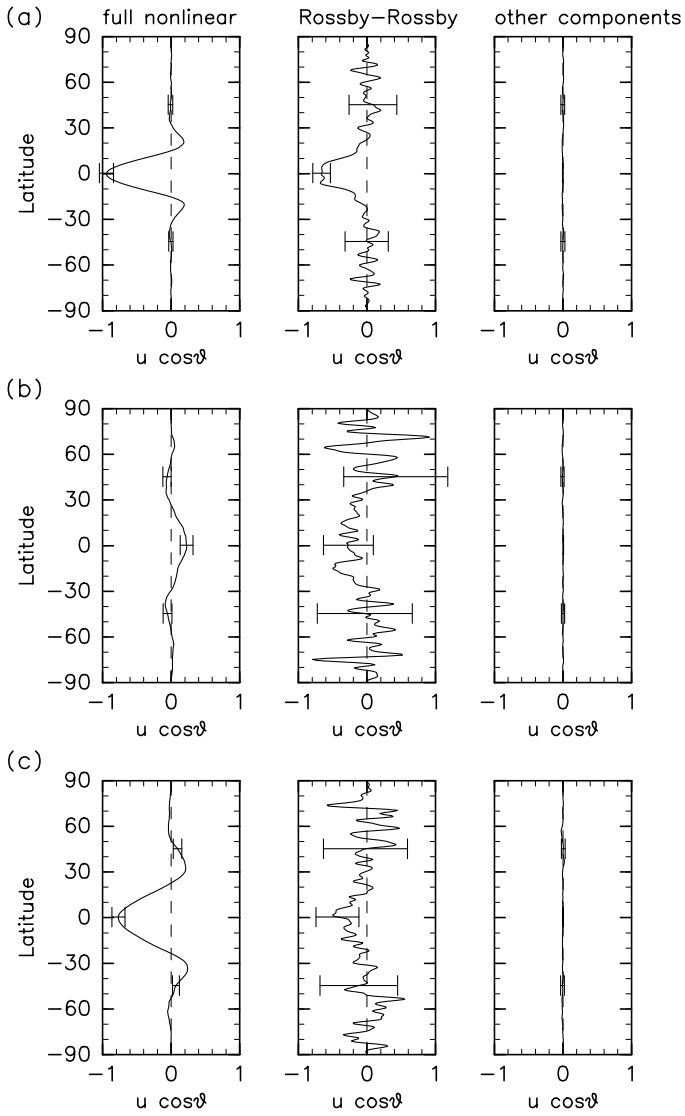

Figure 7: Acceleration of $u\cos\theta$ or $u_2\cos\theta$ between $t = 5$ and 15 without a jet as a basic field. (a) All ensemble members in $\mathrm{Ro} = 0.01$, (b) 50 prograde ensemble members in $\mathrm{Ro} = 0.03$, and (c) 50 retrograde ensemble members in $\mathrm{Ro} = 0.03$ are used. Left panels show the zonal flow acceleration obtained in the full nonlinear model described in Section 2. The middle and right panels present the second-order acceleration induced by the Rossby modes only and the other parts. Error bars show half of standard deviation.

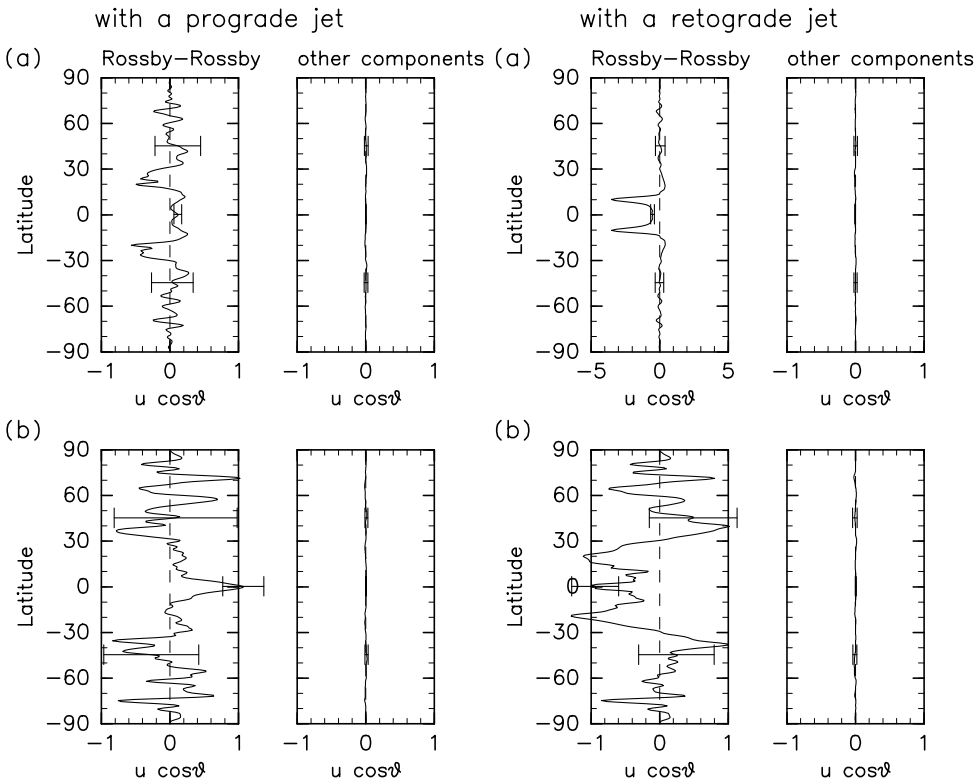

Figure 8: Second-order acceleration of zonal flow with a prograde jet (left panels) and a retrograde jet (right panels). (a) All ensembles members in $\mathrm{Ro} = 0.01$ and (b) 50 prograde ensembles members in $\mathrm{Ro} = 0.03$ are used.

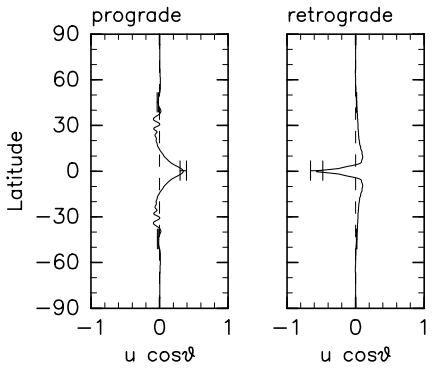

Figure 9: Same as Figure 8(b), except that, here, the contribution of westward-propagating Rossby-gravity modes is extracted.

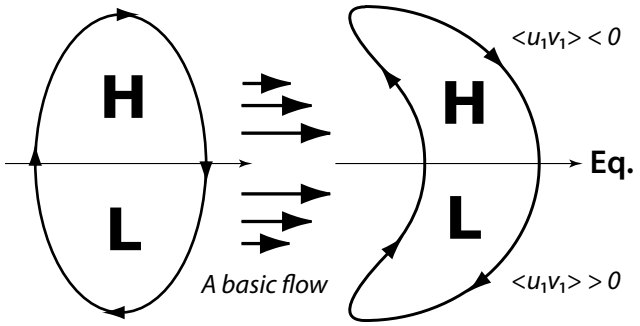

Figure 10: Schematic illustration of the jet amplification mechanism by MRG waves. See text for details.

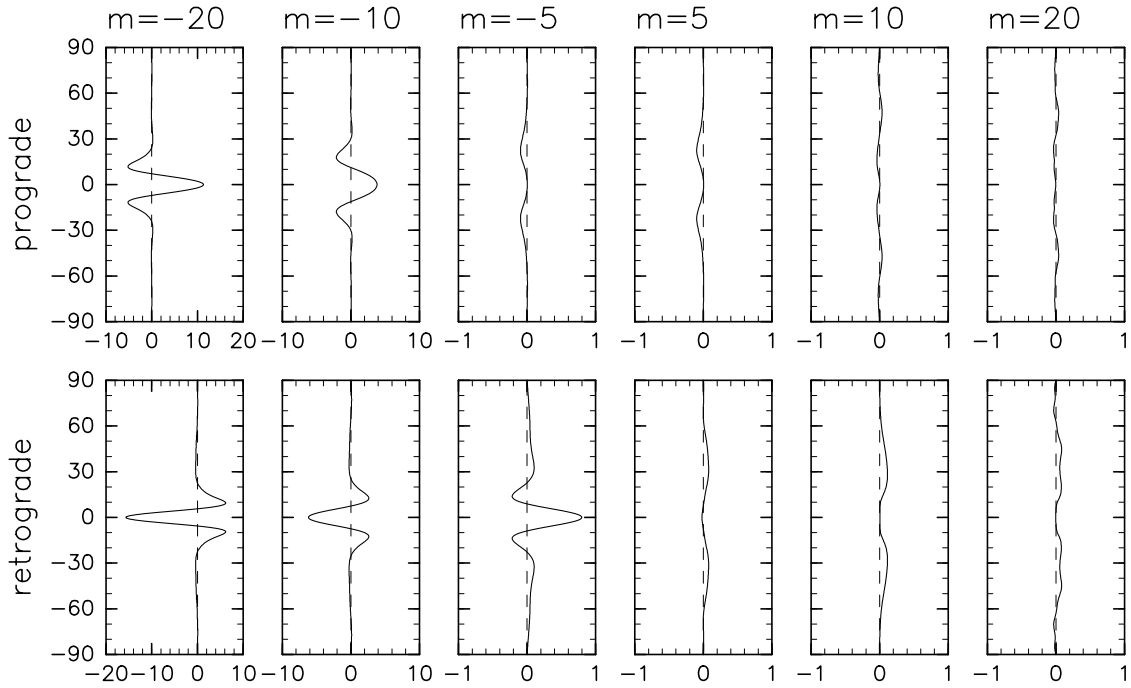

Figure 11: The acceleration of $u_2 \cos\theta$ due to a monochromatic MRG wave. Prograde and retrograde jets are supposed as basic fields in the top and bottom panels, respectively.

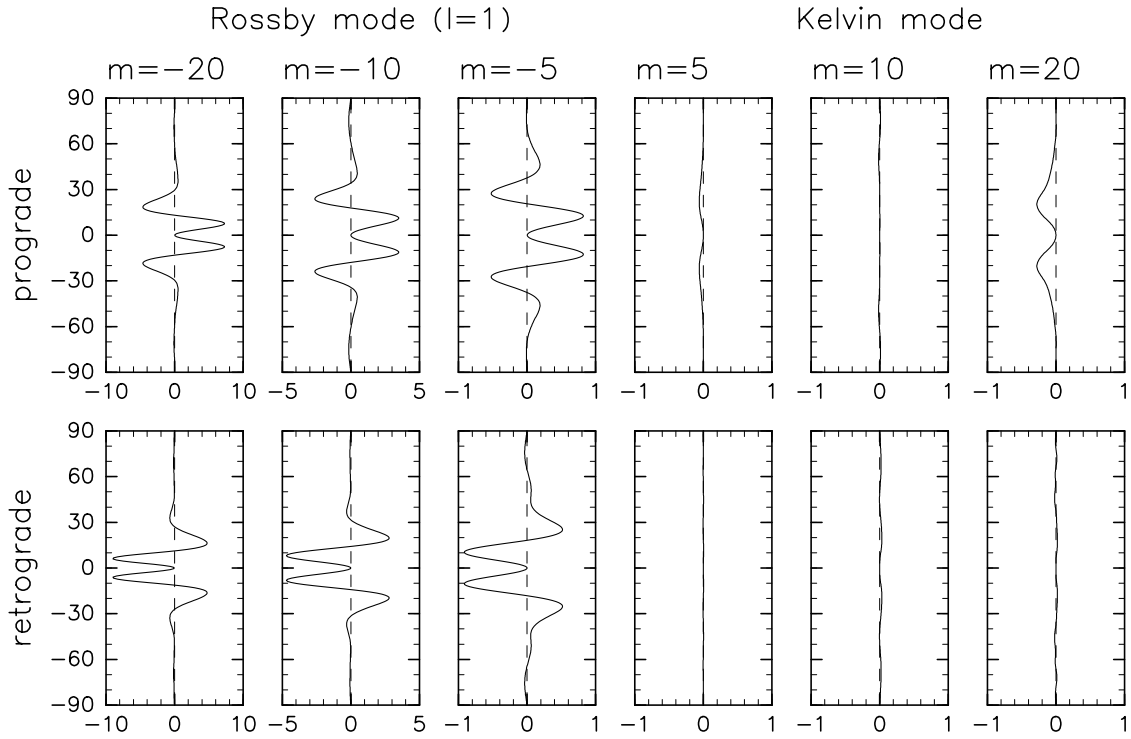

Figure 12: As in Figure 11, but for Kelvin and Rossby waves with the lowest meridional wavenumber.